Biomaterials 158 (2018) 44–55

Contents lists available at ScienceDirect

Biomaterials

journal homepage: www.elsevier.com/locate/biomaterials

Precision design of nanomedicines to restore gemcitabine chemosensitivity for personalized pancreatic ductal adenocarcinoma treatment

Xiao Zhao [a, b, 2], Xiuchao Wang [b, 2], Wei Sun [b, 2, 1], Keman Cheng [a], Hao Qin [a], Xuexiang Han [a], Yu Lin [d], Yongwei Wang [a], Jiayan Lang [a], Ruifang Zhao [a], Xiaowei Zheng [b], Ying Zhao [a], Jian shi [a], Jihui Hao [b], Qing Robert Miao [a, c], Guangjun Nie [a, *], He Ren [b, **]

[a] CAS Key Laboratory for Biomedical Effects of Nanomaterials and Nanosafety, & CAS Center for Excellence in Nanoscience, National Center for Nanoscience and Technology of China, 11 Beiyitiao, Zhongguancun, Beijing, 100190, China
[b] Department of Pancreatic Carcinoma, Tianjin Medical University Cancer Institute and Hospital, National Clinical Research Center of Cancer, Key Laboratory of Cancer Prevention and Therapy, Tianjin, 300060, China
[c] Division of Pediatric Surgery, Department of Surgery, Divisions of Pediatric Pathology, Department of Pathology, Children's Research Institute, Medical College of Wisconsin, Milwaukee, WI, 53226, USA
[d] CAS Key Laboratory of Analytical Chemistry for Living Biosystems, Zhongguancun North First Street 2, 100190, Beijing, PR China

ARTICLE INFO

Article history:
Received 14 September 2017
Received in revised form
18 December 2017
Accepted 18 December 2017
Available online 20 December 2017

Keywords:
Nanocarriers
Gemcitabine
Pancreatic ductal adenocarcinoma
hENT1
RRM2

ABSTRACT

Low chemosensitivity considerably restricts the therapeutic efficacy of gemcitabine (GEM) in pancreatic cancer treatment. Using immunohistochemical evaluation, we investigated that decreased expression of human equilibrative nucleoside transporter-1 (hENT1, which is the major GEM transporter across cell membranes) and increased expression of ribonucleotide reductase subunit 2 (RRM2, which decreases the cytotoxicity of GEM) was associated with low GEM chemosensitivity. To solve these problems, we employed a nanomedicine-based formulation of cationic liposomes for co-delivery of GEM along with siRNA targeting RRM2. Due to the specific endocytic uptake mechanism of nanocarriers and gene-silencing effect of RRM2 siRNA, this nanomedicine formulation significantly increased GEM chemosensitivity in tumor models of genetically engineered Panc1 cells with low hENT1 or high RRM2 expression. Moreover, in a series of patient-derived cancer cells, we demonstrated that the therapeutic benefits of the nanomedicine formulations were associated with the expression levels of hENT1 and RRM2. In summary, we found that the essential factors of GEM chemosensitivity were the expression levels of hENT1 and RRM2, and synthesized nanoformulations can overcome these problems. This unique design of nanomedicine not only provides a universal platform to enhance chemosensitivity but also contributes to the precision design and personalized treatment in nanomedicine.

1. Introduction

Ever since the effective use of aminopterin and nitrogen mustards for cancer treatment in the mid 20th century [1,2], chemotherapy has profoundly influenced the survival of many cancer patients. Despite the successful development of chemotherapeutic agents, one of major hurdles for successful chemotherapy is drug resistance [3]. Resistance after initial drug treatment leads to unsatisfactory chemotherapeutic effects in cancer patients, especially in individuals with cancers of a low resectable rate, such as pancreatic ductal adenocarcinoma (PDAC).

Due to the difficulty of early diagnosis, only 20% of patients with pancreatic cancer are considered surgically resectable [4]. For the other 80% of patients with advanced pancreatic cancer, radiotherapy [5] and recently developed targeted therapy [6] have limited survival benefit; the main treatment scheme remains to be

* Corresponding author.
** Corresponding author.
E-mail addresses: niegj@nanoctr.cn (G. Nie), renhe@tjmuch.com (H. Ren).
[1] Current address: Department of Breast Surgery, Fudan University Shanghai Cancer Center, Cancer Institute, Fudan University Shanghai Cancer Center, Department of Oncology, Shanghai Medical College, Fudan University, P.R. China.
[2] The authors contributed equally to this paper.

https://doi.org/10.1016/j.biomaterials.2017.12.015
0142-9612/

chemotherapy. The median overall survival of patients with metastatic pancreatic cancer is fewer than 7 months, even when patients are treated with the current first-line regimen, gemcitabine (GEM, 2′-deoxy-2′,2′-difluorocytidine, dFdC) [6]. The objective response rate was only 9.4% after GEM single agent treatment in pancreatic cancer patients [6], which is attributed to severe drug resistance against GEM in the majority of patients. Although there are many causes of drug resistance in clinic, including limited vascular accessibility and dense extracellular matrix as drug delivery barriers in the tumor microenvironment, the major cause of drug resistance is the low chemosensitivity of cancer cells *per se* [7–9].

The process of cellular uptake and intracellular metabolism of GEM in cancer cells is complex, and many factors affect GEM cytotoxicity (Fig. S1) [10]. As a pro-drug with high hydrophilicity, GEM penetration across the cell membrane depends on an appropriate transporter. In human cancer cells, human equilibrative nucleoside transporter-1 (hENT1, GenBank accession no. 2030) was identified as the major GEM transporter across cell membranes [11,12]. Once inside the cell, GEM must be converted to its diphosphate (dFdCDP) and triphosphate (dFdCTP) forms. During this transformation, deoxycytidine kinase (dCK, GenBank accession no. 1633) is the rate-limiting enzyme [13–15]. dFdCTP inhibits DNA synthesis by being incorporated into DNA, where it leads to masked chain termination and subsequent apoptosis. Also, dFdCDP can irreversibly inactivate ribonucleotide reductase (RR), which catalyzes the conversion of ribonucleoside diphosphates (NDP) to deoxyribonucleoside diphosphates (dNDP), which is essential for DNA replication [16]. Moreover, it has been reported that overexpression of RR induces high levels of dNTP pools, which can competitively inhibit the incorporation of dFdCTP into DNA, thereby decreasing the cytotoxicity of GEM [17]. Human RR is a dimeric enzyme comprising two subunits, M1 (RRM1, GenBank accession no. 6240) and M2 (RRM2, GenBank accession no. 6241) [18,19]. Although the potential correlation between the expression levels of the four essential proteins in GEM metabolism (hENT1, dCK, RRM1, and RRM2) and GEM chemosensitivity in both pancreatic cancer cells and clinical studies have been reported [20–26], there is still no consensus on the key factors involved in GEM chemosensitivity at present.

Nanocarrier-based drug delivery systems have been devised and evaluated for their ability to deliver therapeutic cargoes (such as drugs and/or siRNA) to overcome drug resistance [27–31]. The solutions based on nanomedicines have been applied as a co-delivery of multiple drugs and/or chemosensitizers to increase local drug concentrations due to passive and/or active tumor target effects. To maximize the clinical benefit of nanomedicines, an in-depth understanding of the mechanisms by which tumors resist drugs is critical for the customized design of nanocarriers and identification of the patient subpopulations responding to a given nanomedicine. Herein, we describe a precise design to increase GEM chemosensitivity in pancreatic cancer. Our strategy began with a rigorous statistical analysis of clinical data to determine that the key factors responsible for low GEM chemosensitivity in North China were low hENT1 and high RRM2 expression, followed by the design of functional nanocarriers directly address the clinical discovery. The delivery of GEM by nanocarriers and endocytosis into cancer cells could overcome the low chemosensitivity caused by low hENT1 expression. In addition, the co-delivery with siRNA against RRM2 would enhance the chemosensitivity of GEM in cancer cells with high RRM2 expression. Next, genetically engineered pancreatic cancer cell lines with different expression levels of those key factors were utilized to assess the therapeutic efficacy of the nanomedicine. Finally, the antitumor efficacy of GEM and the nanomedicine formulations were evaluated in primary patient-derived pancreatic cancer cells. The different levels of therapeutic benefit revealed the importance and necessity of personalized application of nanomedicine.

2. Materials and methods

2.1. Patient cohort and clinical treatment

The use of human samples was approved by the Ethics Committee of Tianjin Medical University Cancer Institute and Hospital and followed the ethical guideline. We obtained the informed consent from all subjects. We retrospectively enrolled all patients who received a radical resection with a pathologically confirmed diagnosis of pancreatic ductal adenocarcinoma and were treated at Tianjin Cancer Hospital from December 2009 to January 2013. The follow-ups for final analysis ended on June 30, 2015. Patients with at least one of the following conditions were excluded: (1) patients who received neoadjuvant chemotherapy, chemoradiotherapy, or non-GEM-based chemotherapy; (2) patients with macroscopically incomplete resection; (3) patients with a history of another major cancer; (4) patients who died within one month after the operation or due to non-cancer related causes. The patients received at least three cycles of GEM-based chemotherapy after operation. GEM was delivered by a 30-min intravenous infusion at a dose of 1000 mg per square meter of body surface area weekly for two weeks followed, by one week intervals, then for two weeks in a subsequent three-week course.

2.2. Immunohistochemistry

For IHC analysis of tissue microarray, anti-hENT1 mouse monoclonal antibody (sc-377283, 1:100, Santa Cruz, USA), anti-dCK rabbit polyclonal antibody (ab151966, 1:500, Abcam, UK), anti-RRM1 rabbit monoclonal antibody (ab133690, 1:350, Abcam, UK), and anti-RRM2 mouse monoclonal antibody (ab57653, 1:500, Abcam, UK) were used to determine the levels of protein expression of hENT1, dCK, RRM1 and RRM2, respectively. IHC slides were independently graded by two pathologists, who were blinded to patient outcomes. Discordant cases were assessed by a third pathologist, and a consensus was reached.

Membrane and cytoplasmic staining for hENT1 were regarded as positive. Cytoplasmic staining for dCK, RRM1 and RRM2 was regarded as positive. Immunoreactivity was scored semi-quantitatively according to the intensity and extent of tumor cell staining. The intensity of tumor cells staining was scored as 0 = negative, 1 = low, 2 = medium and 3 = high. The extent of staining was scored as 0 = 0%–5% staining, 1 = 5%–25% staining, 2 = 26%–50% staining and 3 = 51%–100% staining. The final score was determined by multiplying the scores of intensity with the extent of staining, in the range of 0–9. Final scores of less than 1 were considered negative (−), 1–2 as low staining (+), 3–4 as medium staining (++) and 6–9 as high staining (+++).

2.3. Synthesis of nanoformulations

The DOTAP-based cationic liposome nanoparticles (approved by the US Food and Drug Administration for clinical trials, NCT00059605) were prepared by a lipid film method. Briefly, a 15 μmol lipid mixture of DOTAP (LP-R4-117, Ruixi Biological Technology Co., China), dioleoyl-phosphatidylethanolamine (DOPE, LP-R4-069, Ruixi Biological Technology Co., China), cholesterol (Chol, 121530, JK Chemical, China) and distearoyl-phosphatidylethanolamine-methyl-polyethyleneglycol conjugate-2000 (DSPE-mPEG2000, LP-R4-039, Ruixi Biological Technology Co., China) at a molar ratio of 8:3:8:1 was dissolved in 10 ml

dichloromethane, and dried into a thin film followed by a hydration process with 10 ml double distilled water in a water bath at 50 °C to form multilamellar vesicles (MLV). For NP-GEM synthesis, 60 mg GEM (BIFK0023, JK Chemical, China) was added into the hydration solution. The resulting MLV were then extruded using a LipoFast mini extruder (Avestin, Canada) through a polycarbonate membrane of 0.2 μm with 5 cycles to form large unilamellar vesicles (LUVs). For NP-GEM preparation, the LUVs were centrifuged through a 30 kD ultrafiltration centrifuge tube (Millipore, USA) to remove the un-encapsulated GEM. The NP-GEM was resuspended in 10 ml double distilled water. After demulsification and HPLC analysis for GEM, the encapsulation efficacy was determined to be 15.2% using the formula $R = a/b \times 100\%$, where a is the GEM amount in NP-GEM after demulsification and b is the initially added GEM amount. When the NP and NP-GEM were used to absorb siRNA, the nanoparticle solution was combined with siRNA at a siRNA:DOTAP mass ratio of 0.628:1 and then incubated for 20 min at room temperature. There were 1030 μg lipids, 912 μg GEM and 264 μg siRNA in 1 ml NP-GEM-siRNA in the final preparation.

2.4. Characterization of nanoformulations

For morphology measurements, the nanoparticles were deposited on a carbon-coated copper grid, following by negative staining with 2% uranyl acetate and examination with a transmission electron microscope (TEM, JEM-200CX, Japan). For size distribution and zeta potential measurements, the dynamic light scattering (DLS) was estimated using a Zetasizer Nano ZS90 (Malvern Instruments, UK) with 90° optics and a He–Ne Laser (4.0 mW, 633 nm). For the electromobility shift assay, DNA (pEGFP-N1 plasmid) was mixed with NP-GEM at different mass ratios of DNA:DOTAP for 15 min at room temperature. The mixture was analyzed by gel electrophoresis using a 1% agarose gel for DNA, stained with SYBR and visualized under a UV light.

2.5. In vivo characterization of NP-absorbed siRNA

For circulation experiments, 66 μg Cy3-sicon was adsorbed onto the surface of NP-GEM (NP-GEM-Cy3-sicon). Cy3-sicon and NP-GEM-Cy3-con were injected into the tail veins of female 4-week old nu/nu mice. Mice were imaged at different time intervals using the Maestro™ 2 imaging system (CRI, USA). In addition, blood was drawn at different time intervals after injection and Cy3-siRNA fluorescence intensity was measured using the Infinite M200 microplate reader (TECAN, Switzerland). To generate a conversion formula between siRNA quality and fluorescence intensity in blood, a standard curve using blood from normal mice injected with known amounts of fluorescent siRNA was established.

For tumor targeting experiments, tumor-bearing mice were generated by injecting 5×10^6 Panc1 cells subcutaneously into the right flank. After injection with NP-GEM-Cy3-sicon, organs and tumors were imaged *ex vivo* using the Maestro 2 imaging system. To determine the major percentage of the injected dose accumulated in the organs and tumors, the tissues were pulverized under liquid nitrogen and homogenized in 10 Mm Tris buffer with 1% sodium dodecyl sulfate at 95 °C for 10 min and centrifuged at 14,000 g. The fluorescence intensity of the lysate was measured using an Infinite M200 microplate reader. The standard curve for each organ was also generated using the organs and tumors from un-injected animals.

2.6. Antitumor efficacy in vivo

All animal experiments were reviewed by the animal ethics committee of National Center of Nanoscience and Technology, China and followed the guideline. All animals were obtained from Vital River Laboratory Animal Technology Co., China. 5×10^6 transfected Panc1 cells were subcutaneously injected into the right flank of female 4-week old nu/nu mice (5 mice/group). When the tumor volume reached about 80 mm^3, the mice were randomly allocated to the different experimental group and different drug formulations (containing 11.4 mg/kg of GEM and/or 3.3 mg/kg of siRNA) were injected into the tail vein. The investigator was not blinded to the group allocation. During the treatment, tumor sizes were measured, and tumor volumes were calculated using formula $V = (1/2)ab^2$, where a is the tumor's long axis and b is the short axis. Mice with tumor implants were euthanized 20 days after drug treatment, and the tumor xenografts were excised and weighed. The tumor inhibition rates were calculated using the formula $R = (1\text{-}a/b) \times 100\%$, where a is the mean tumor mass of the treatment group, and b is the mean tumor mass of the matching saline group.

2.7. Statistical analysis

Kaplan-Meier curves were used to analyze the survival of patients with different expression levels of the different proteins, and the log-rank test was used to obtain a *P*-value for the significance of Kaplan-Meier curves' divergence. Univariate Cox proportional hazards regression model was used to identify predictors of prognosis in various patient demographics and clinical characteristics. Significant clinical and demographic variables and four variables of protein expression (hENT1, dCK, RRM1, and RRM2) were then added into the final model for backward selection of the multivariate Cox proportional hazards regression model, to identify independent prognostic factors. Except for clinical analysis and *in vivo* experiments, all the experiments were replicated 3 times. The data is presented as mean ± s.d., and the two-sided Student's t-test for unpaired data was used to compare mean values. Analyses were performed using the SPSS17.0 statistical analysis software. A *P*-value of <0.05 was considered statistically significant.

3. Results

3.1. Identification of a correlation between low hENT1 or high RRM2 protein expression and poor prognosis in PDAC patients receiving GEM treatment

To determine the key factors associated with clinical GEM chemosensitivity, we first used immunohistochemistry (IHC) to examine the expression level of four proteins (hENT1, dCK, RRM1 and RRM2) in a tissue microarray consisting of 96 human PDAC specimens, who received at least three cycles of GEM-based chemotherapy after radical resection. Representative images of patient samples stained for the four proteins are shown in Fig. S2. According to our scoring system, the expression levels were divided into two groups: high expression (++ and +++) and low expression (- and +). Using Kaplan-Meier curves for survival analysis, we found that the patients with low hENT1 protein expression ($hENT1^{low}$) had a significantly poor overall survival (OS) and relapse free survival (RFS) than those patients with high hENT1 protein expression (Fig. 1A and B). The patients with high RRM2 protein expression ($RRM2^{high}$) also had significantly worse OS and RFS than those with low RRM2 protein expression (Fig. 1A and B). In addition, multivariate Cox regression analysis identified that the expression of hENT1 and RRM2 protein were significantly independent prognostic factors for OS (Table S1). Taken together, the clinical data suggest that low hENT1 and high RRM2 protein expression are the critical factors correlated with poor GEM chemosensitivity in pancreatic cancer patients.

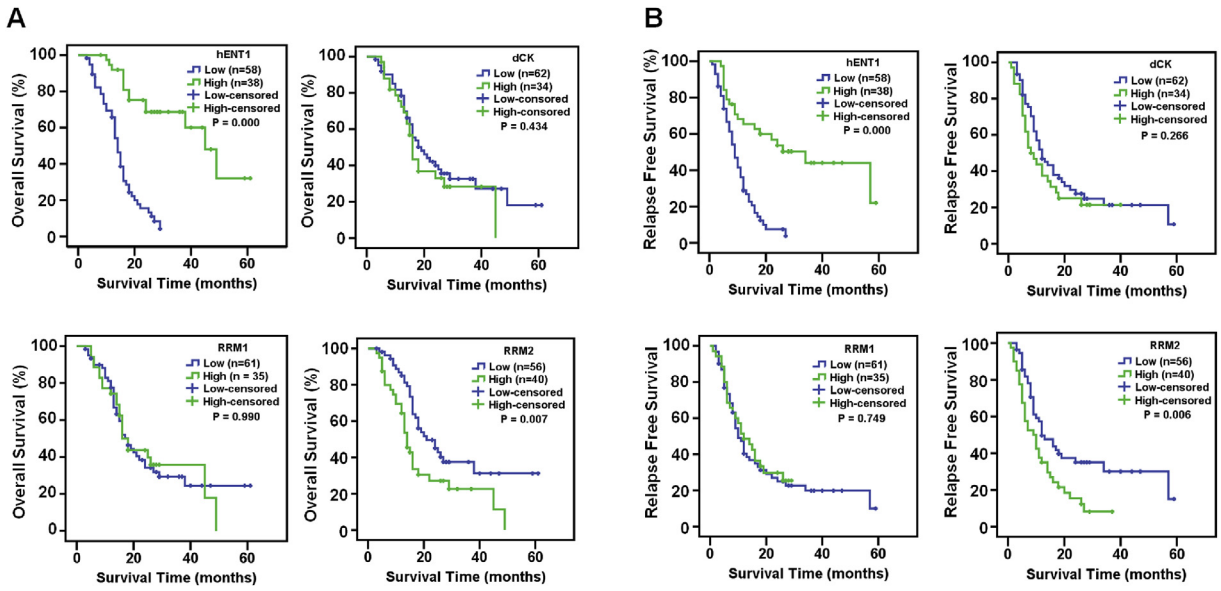

Fig. 1. Identification of the clinical key factors associated with GEM chemosensitivity in pancreatic cancer patients. (A) and **(B)** Kaplan-Meier curves were used for survival analysis for (A) OS and (B) RFS according to the different expression levels of the four proteins. There are censored data in cases of a lack of monitoring. The *P* values were obtained using the log-rank test.

3.2. Design and synthesis of nanomedicine to increase GEM chemosensitivity

To precisely design nanotherapeutics specifically for GEM chemosensitivity in pancreatic cancer treatment, a nanocarrier with features specifically targeting hENT1^{low} or RRM2^{high} was created as shown in Fig. 2A. Dioleoyl-trimethylammonium propane (DOTAP)-based cationic liposomal nanoparticles (NP) were used to encapsulate GEM into the carrier's hydrophilic core (NP-GEM). To specifically deplete RRM2 expression in tumor tissues, negatively charged siRNA targeting RRM2 (siRRM2) was absorbed onto the surface of the cationic nanoparticles by electrostatic forces. The

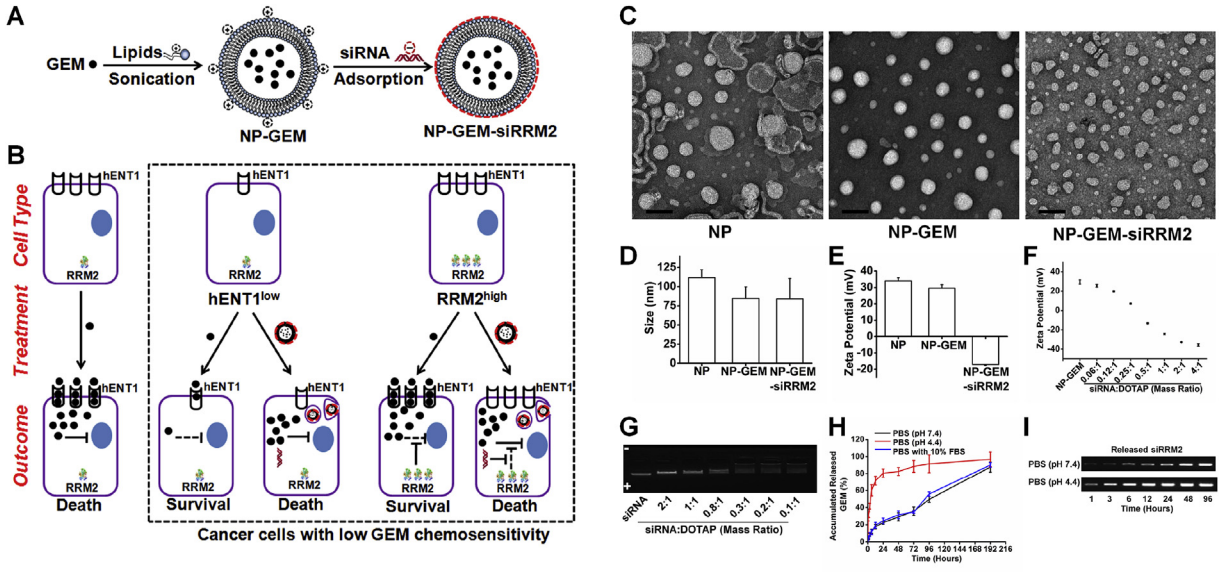

Fig. 2. Design principle of nanoformulations to enhance GEM chemosensitivity and characterization of the nanocarriers with different components. **(A)** Synthesis of the nanoformulations to simultaneously delivery GEM and siRRM2. The DOTAP-based cationic liposome was assembled by a lipid film dispersion method, and encapsulated GEM into its hydrophilic core in the preparation process (NP-GEM). The negatively charged siRRM2 was then absorbed onto the surface of nanoparticles by electrostatic forces (NP-GEM-siRRM2). **(B)** Enhancement of chemosensitivity by NP-GEM-siRRM2 related to GEM in pancreatic cancer cells with low hENT1 protein expression (hENT1^{low}) or high RRM2 protein expression (RRM2^{high}). Due to a lack of uptake mechanism in hENT1^{low} cancer cells, GEM cannot effectively enter cells to induce apoptosis. This uptake barrier can be bypassed by encapsulating GEM into nanocarriers that enter the cell *via* endocytosis. In addition, the siRRM2, simultaneously delivered into tumor cells, will aid GEM in overcoming the low chemosensitivity caused by excessive RRM2 expression in RRM2^{high} cancer cells. **(C)** TEM images of NP, NP-GEM and NP-GEM-siRRM2. **(D)** The particle sizes of NP, NP-GEM and NP-GEM-siRRM2. **(E)** The zeta potential of NP, NP-GEM and NP-GEM-siRRM2. **(F)** The zeta potential changes of NP-GEM after surface absorption with sicon under different mass ratios of siRNA:DOTAP. **(G)** The electromobility shift assay of siRNA when they were mixed with NP-GEM in different mass ratios of siRNA:DOTAP. **(H)** The drug release profiles of NP-GEM-siRRM2 at different PBS solutions (pH 4.4, 7.4 or 7.4 with 10% FBS). **(I)** The siRRM2 release profiles of NP-GEM-siRRM2 at different PBS solutions (pH 4.4 or 7.4) over times were examined by gel electrophoresis.

main strategy of this design system enables the efficient, endocytic delivery of GEM into hENT1^{low} cancer cells, which originally lack of uptake mechanism on the cell membrane due to low hENT1 expression [20,21]. This endocytic delivery potentially overcomes the low chemosensitivity caused by hENT1^{low}. In addition, the siRRM2 that are simultaneously absorbed and delivered into cells will assist GEM in evading the low chemosensitivity caused by excessive RRM2 expression in RRM2^{high} cancer cells (Fig. 2B).

The transmission electron microscopy (TEM) data demonstrated that the liposomal nanoparticles were well dispersed with a defined spherical structure (Fig. 2C). The addition of GEM into the nanoparticles led to assembly into even more uniform spherical nanoparticles (NP-GEM; Fig. 2C). According to DLS measurements, the average hydrodynamic diameters of NP and NP-GEM were 111.9 ± 10.1 and 85.4 ± 15.3 nm, respectively (Fig. 2D). The zeta potential of NP was 34 ± 2.1 mV, due to the cationic lipids, and changed to 29.5 ± 2.1 mV after GEM encapsulation (Fig. 2E). The GEM encapsulation did not significantly influence the positive charge and the nucleic acid binding capacity of the liposomes. Next, we examined the nucleic acid-binding capacity of NP-GEM. With increased mass ratios of siRNA:DOTAP from 0.06:1 to 4:1, the zeta potential of NP-GEM changed from 25.5 to −35.7 mV (Fig. 2F). In addition, the result of electromobility shift assay titration experiments showed that the siRNA was fully neutralized, i.e., no addition mobility was observed, when the siRNA:DOTAP ratio was lower than 0.3:1 (mass ratio; Fig. 2G). These results indicate that NP-GEM possess a strong nucleic acid-binding capacity. The nanocarriers absorbed siRRM2 at a final therapeutic dose of 0.628:1 of siRRM2:DOTAP (mass ratio). Compared to NP-GEM, the siRRM2-absorped NP-GEM (NP-GEM-siRRM2) had a slightly irregular surface after absorbing siRNA (Fig. 2C), a minor difference in size distribution (84.1 ± 26.6 nm) (Fig. 2D), and a zeta potential that radically changed to -17.1 ± 0.6 mV, due to the siRRM2 binding (Fig. 2E).

Next, we measured the *in vitro* release profiles of NP-GEM-siRRM2 at different PBS solutions (pH 4.4, 7.4 or 7.4 with 10% FBS). The releases of GEM at PBS (pH 7.4) or PBS with 10% FBS were slow and sustained, and only about 20% of GEM was accumulatively released within 12 h (Fig. 2H). However, the accumulative drug release was much faster at acidic PBS solution (pH 4.4), which is similar to that of the lysosomes, with 82.4% GEM being released within the first 48 h (Fig. 2H). The release of siRRM2 was also faster at acidic PBS solution than that at PBS with pH 7.4 (Fig. 2I). The underlying mechanism for the accelerated release of cargoes at pH 4.4 may associated with the transition of the DOPE liposomes from a bilayer structure to a hexagonal arrangement under pH 4.4, which accelerates the liposomal disassembly and drug release [32].

3.3. Characterization of siRNA-delivery ability and knockdown efficiency in vitro and in vivo

Next we further studied if and the extent to which NP-absorbed siRNA can be effectively delivered into cells and knockdown gene expression both *in vitro* and *in vivo*. To analyze the siRNA-delivery efficacy across cell membranes, the fluorescence intensity of Panc1 cells was measured by flow cytometry after incubation with Cy3-labeled random control siRNA (sicon)-absorbed NP-GEM (NP-GEM-Cy3-sicon) for different time intervals. As shown in Fig. 3A, the fluorescence intensity of cells gradually increased with prolonged incubation time, indicating that more and more siRNA was bound on to the cell membrane or delivered into cells by our nanocarriers, at least in the first 6 h. To examine the intracellular localization of siRNA, NP-GEM-sicon was labeled with FAM in green fluorescence (NP-GEM-FAM-sicon), and the lysosomes in cells were stained into red fluorescence. Panc1 cells treated with this conjugate were observed under a scanning confocal laser microscope. At 0.5 and 3 h, the membrane localization of most fluorescence signal indicated that most NP-GEM-FAM-sicon were bound to the cell membrane. With prolonged incubation time (6 h and 12 h), NP-GEM-FAM-sicon fluorescence signal gradually shifted from the cell membrane to the lysosomal compartment, as shown by an apparent overlay of green and red fluorescence. After 24 h incubation, payloads were released to the cytoplasm as shown by the separation of the green and red fluorescence signals (Fig. 3B). We selected GAPDH as a target gene to analyze the knockdown efficiency *in vitro*. As shown in Fig. 3C, treatment with siRNA against GAPDH (siGAPDH)-absorbed onto NP-GEM (NP-GEM-siGAPDH) led to a significant knockdown (63%) of GAPDH protein *in vitro*, which was slightly lower than that elicited by transfection with Lipofectamine 2000 (77%).

For siRNA applications *in vivo*, an ideal carrier should protect siRNA from nuclease degradation in the bloodstream, thus extending the circulating time of siRNA. To compare the circulating time of siRNA with or without delivery by our nanoformulations, naked Cy3-sicon or NP-GEM-Cy3-sicon were injected (*i.v.*) into mice. We quantified the fluorescent sicon circulating in the bloodstream at different time intervals. The results show that there was significantly more circulating sicon in the NP-GEM-Cy3-sicon group than that in the Cy3-sicon group at almost every time point. Compared to the Cy3-sicon group, an over 3.8-fold increase in the circulating half-life of NP-GEM-Cy3-sicon group was observed (13 *vs.* 63 min; Fig. 3D). In addition, the *in vivo* fluorescence images show that most of the naked Cy3-sicon was cleared through the kidney, as indicated by the accumulation of fluorescent siRNA in the bladder (Fig. S3). Meanwhile, NP-GEM-Cy3-sicon mainly accumulated in the liver, likely due to uptake by the reticuloendothelial system (RES) (Fig. S3).

To assess organ distribution and tumor-penetration of siRNA to established tumors, naked Cy3-sicon or NP-GEM-Cy3-sicon were injected into mice bearing subcutaneous human pancreatic tumors (Panc1 xenografts), followed by a quantitative evaluation of fluorescent sicon distribution in organs at different time points. As shown in Fig. 3E and F, more sicon accumulated in all the major organs investigated in the NP-GEM-Cy3-sicon group than in the Cy3-sicon group. This enhanced organ distribution is likely attributed to the longer circulation time of NP-GEM-Cy3-sicon. Consistent with the *in vivo* results, the *ex vivo* organ fluorescence images indicate that naked Cy3-sicon was preferentially distributed to or metabolized in the kidney, while NP-GEM-Cy3-sicon accumulated in the liver (Fig. 3E and F). In addition, there were small fractions of NP-GEM-Cy3-sicon in the spleen, likely due to RES uptake, and the lung, the first capillary bed following intravenous injection. Most importantly, we found a clear increase in tumor-accumulation in the NP-GEM-Cy3-sicon group compared to the Cy3-sicon group (7.1% vs. 3.5% injected dose/gram tissue 2 h after injection) (Fig. 3E and F). The enhanced fluorescence intensity of tumor tissue also exhibits the better tumor targeting of NP-GEM-Cy3-sicon, compared to naked Cy3-sicon (Fig. 3G). These results show that NP-GEM-Cy3-sicon can preferentially accumulate in tumors after intravenous injection. Finally, the results of immunoblotting of tumor tissues and probing for GAPDH showed an over 70% knockdown efficacy in the NP-GEM-siGAPDH group compared to the NP-GEM-sicon group (Fig. 3H). All of these results indicate that our nanoformulation is an effective siRNA carrier for tumoral gene silencing *in vivo*.

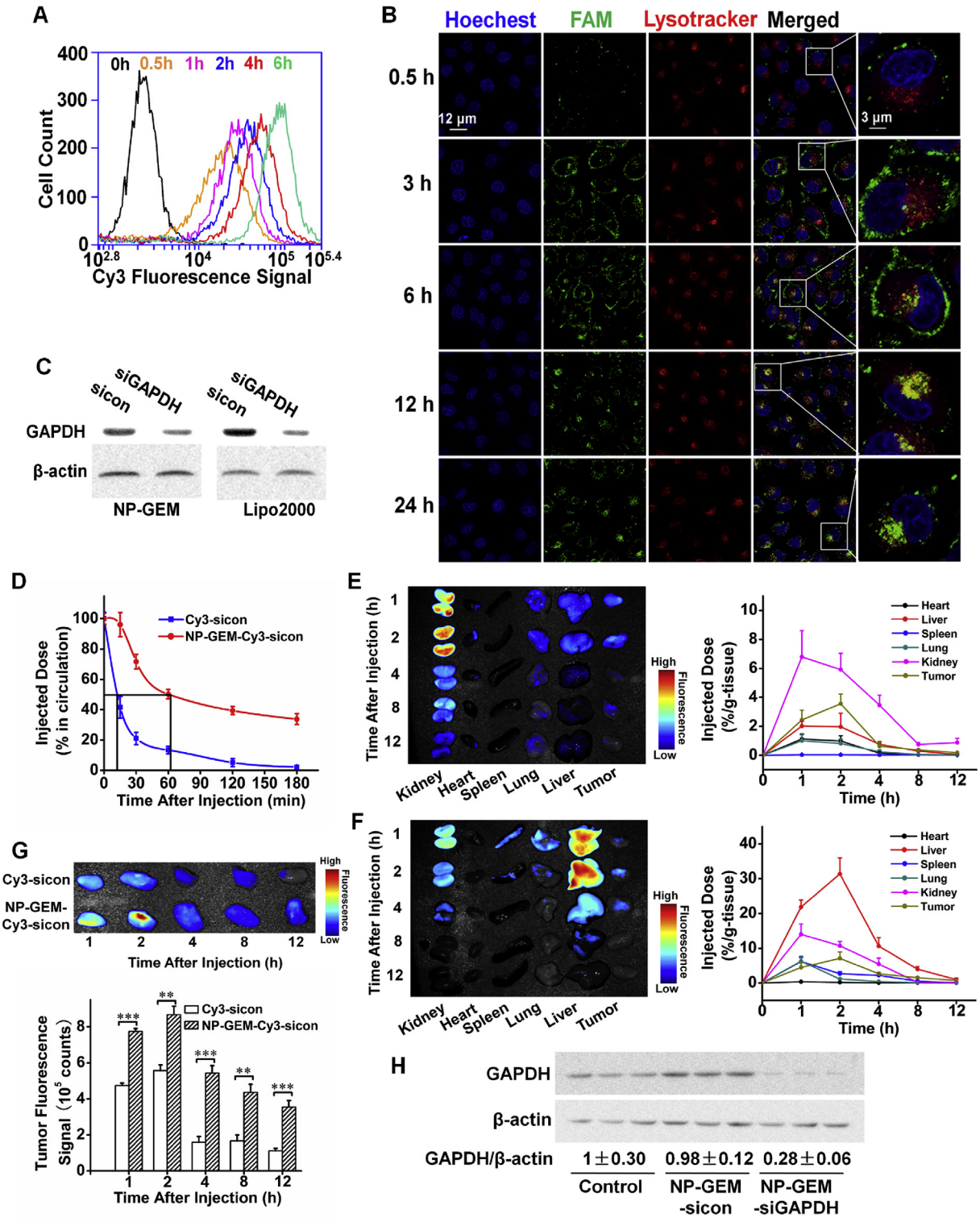

Fig. 3. Characterization of siRNA-delivery capacity and knockdown efficiency *in vitro* and *in vivo*. **(A)** Cellular uptake efficacy of siRNA delivered by nanoparticles. Panc1 cells were incubated with NP-GEM-Cy3-sicon for the indicated durations, and the fluorescence intensity of cells was measured by flow cytometry. **(B)** Observation of intracellular location of siRNA. Sicon was labeled with FAM, and Panc1 cells treated with NP-GEM-FAM-sicon for different time intervals were observed by confocal microscopy. Cell nuclei (blue) were stained by Hoechst 33342, and the lysosomes were stained with LysoTracker Red. **(C)** The knockdown effects *in vitro*. The knockdown efficacy of GAPDH in Panc1 cells after treatment with NP-GEM-siGAPDH was detected by immunoblotting. Lipofectamine 2000 (Lipo2000) was used as a positive control. **(D)** Quantification of sicon circulating in the bloodstream of mice at various time points after intravenous injection of naked Cy3-sicon and NP-GEM-Cy3-sicon. The half-lives in circulation were calculated from these data (black lines). **(E, F)** *In vivo* biodistribution of (B) naked Cy3-sicon and (C) NP-GEM-Cy3-sicon, upon intravenous administration. Mice bearing subcutaneous Panc1 xenografts were injected intravenously with naked Cy3-sicon and NP-GEM-Cy3-sicon. After different time intervals, the major organs and tumors were harvested and imaged for siRNA fluorescence. **(G)** Tumor targeting effect *in vivo*. The tumors in panel E and F were imaged for siRNA fluorescence and the fluorescence intensities were quantified. **(H)** The siRNA knockdown efficiency *in vivo*. Mice bearing subcutaneous Panc1 xenografts were injected intravenously with saline, NP-GEM-sicon or NP-GEM-siGAPDH. After 48 h, tumors were harvested, and proteins were extracted and estimated by immunoblotting. $^{**}P < .01$, $^{***}P < .001$.

3.4. NP-GEM-sicon treatment elicits enhanced antitumor effects in pancreatic cancer cells and xenografts with low hENT1 protein expression

First, we employed a lentiviral system to create two stable Panc1 cell lines with hENT1-specfic shRNA expression (Panc1-shENT1#1 and Panc1-shENT1#2). Random shRNA was used as a negative control (Panc1-shcon). Immunoblotting confirmed stable shRNA expression in Panc1-shENT1#1 and Panc1-shENT1#2 cells (Fig. S4). Next, the engineered cells with differing expression levels of hENT1 were treated with GEM or NP-GEM-sicon. As shown in Fig. 4A, after 48 h GEM treatment, there was a significant difference in apoptotic cell rates between Panc1-shENT1#1 or Panc1-shENT1#2 and the control (15.2% or 15.8% *vs.* 23.7%). However, we did not detect such a significant difference after NP-GEM-sicon treatment. Unlike GEM treatment, NP-GEM-sicon treatment resulted in significant amount of cell apoptosis in Panc1-shENT1#1 and Panc1-shENT1#2 cells. To investigate whether the apoptosis rates result from differing efficiencies of GEM delivery, we used high performance liquid chromatography (HPLC) to analyze the triphosphate form of GEM, dFdCTP in the cell lysates at different time intervals after 50 μM GEM and NP-GEM-sicon treatments. As shown in Fig. 4B, there was significantly less dFdCTP in the cell lysates of Panc1-shENT1#1 and Panc1-shENT1#2 cells than that of Panc1-shcon cells after GEM treatment. By contrast, the intracellular levels of dFdCTP after NP-GEM-sicon treatment in each group were similar (Fig. 4B). These results suggest that hENT1^{low} is an obstacle attenuating GEM accumulation in cells and the endocytic delivery NP-GEM-sicon into cells can overcome the hENT1^{low} caused blockage.

Since the confocal microscopy experiments (Fig. 3B) indicated that NP-GEM-sicon enters cells *via* lysosome-dependent endocytosis, we further investigated the endocytic pathways involved. Panc1 cells were pretreated with ethylisopropylamiloride (EIPA, an inhibitor of macropinocytosis), nystatin (an inhibitor for caveolae-mediated endocytosis) or chlorpromazine (an inhibitor for clathrin-mediated endocytosis), or incubated at 4 °C. The cells were then incubated with NP-GEM-Cy3-sicon for 3 h, and the mean fluorescence intensities of cells were measured using flow

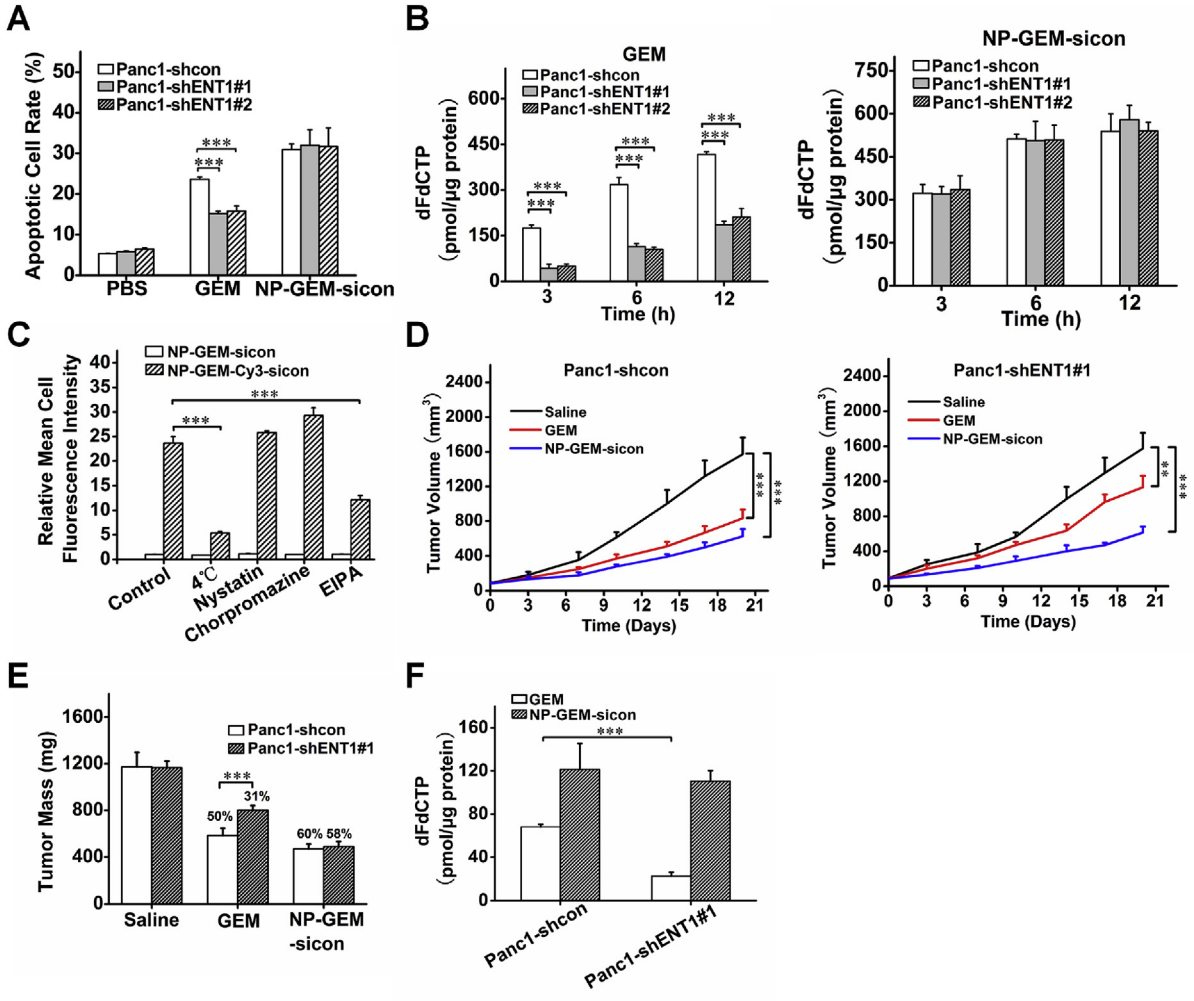

Fig. 4. The enhanced chemosensitivity of NP-GEM-sicon, as compared to GEM, in pancreatic cancer cells and xenografts with hENT1^{low}. **(A)** The apoptotic cell rate of different Panc1 cell phenotypes after 48 h treatment with different drug formulations. **(B)** Analysis of triphosphate form of GEM, dFdCTP in the cell lysates at different time intervals after GEM and NP-GEM-sicon treatments. The dFdCTP concentration was measured by HPLC and normalized to total protein concentration. **(C)** Analysis of the endocytosis pathway of NP-GEM-sicon. sicon was labeled with Cy3. Panc1 cells were incubated at 4 °C or pre-treated with different endocytosis inhibitors, and then incubated with NP-GEM-Cy3-sicon. After 3 h, the mean fluorescence intensity of cells was measured using flow cytometry. **(D, E)** The antitumor effects *in vivo*. Mice (n = 5) bearing subcutaneous xenografts of Panc1-shcon or Panc1-shENT1#1 were treated with different drug formulations once every 3 days for 20 days (D). The tumor volume curves were recorded (E). Mice were sacrificed at day 20, and tumors were removed and weighed. The inset numbers were the tumor inhibitory rates related to saline group. **(F)** Analysis of the dFdCTP levels in tumor tissue lysates using HPLC. $^{*}P < .05$, $^{**}P < .01$, $^{***}P < .001$.

cytometry. The results of this experiment show that pretreatment with EIPA or incubation at 4 °C significantly decrease the mean fluorescence intensity of cells treated by NP-GEM-Cy3-sicon, which we did not observe in nystatin or chlorpromazine pretreated groups (Fig. 4C). These results demonstrate that NP-GEM-sicon was endocytosed into cells mainly *via* macropinocytosis.

We next tested whether our nanoformulations can enhance GEM chemosensitivity in established human pancreatic cancer xenografts with hENT1^{low} *in vivo*. Mice bearing subcutaneous Panc1-shENT1$^{\#}$1 and Panc1-shcon tumors were injected intravenously with saline, GEM or NP-GEM-sicon once every 3 days for 20 days. Compared to saline, administration of GEM resulted in suppression of tumor growth in Panc1-shcon xenografts. However, the inhibitory effect of GEM on tumor growth was significantly weaker in Panc1-shENT1$^{\#}$1 xenografts than in Panc1-shcon xenografts (Fig. 4D). At day 20, treatment with GEM inhibited tumor growth by 50% in Panc1-shcon tumors and 31% in Panc1-shENT1$^{\#}$1 tumors (Fig. 4E and Fig. S5), and HPLC results in Fig. 4F showed the significantly lower level of dFdCTP in Panc1-shENT1$^{\#}$1 xenografts as compared to Panc1-shcon xenografts. In contrast, NP-GEM-sicon treatment achieved the similar tumor inhibitory effects and dFdCTP levels of tumor lysates in both groups (Fig. 4E and F). These data demonstrate that GEM delivery by NP-sicon can overcome the low GEM chemosensitivity in cancer cells with hENT1^{low} *in vivo*.

3.5. Co-delivery of siRRM2 significantly enhances the antitumor effects of NP-GEM-sicon in pancreatic cancer cells and xenografts with RRM2^{high}

A stable RRM2-overexpression Panc1 cell line (Panc1-RRM2) was generated using a lentiviral system (Fig. S6). The empty viral vector was used as a negative control (Panc1-con). Next, we measured the apoptosis frequencies of Panc1-con and Panc1-RRM2 cells after different drug formulation treatment. NP-siRRM2 treatment alone did not induce significant apoptosis in either Panc1-con or Panc1-RRM2 cells. Although NP-GEM-sicon treatment induced about 27.6% apoptosis in Panc1-con cells, the apoptosis frequency was significantly lower (12.4%) in Panc1-RRM2 cells treated with NP-GEM-sicon (Fig. 5A). Importantly, NP-GEM-siRRM2 treatment induced apoptosis in Panc1-RRM2 cells to a similar level as that in Panc1-con cells (26.9% *vs.* 27.9%) (Fig. 5A). The immunoblotting confirmed the decreased RRM2 protein levels after NP-siRRM2 and NP-GEM-siRRM2 treatments (Fig. 5B).

We next evaluated the antitumor effects of NP-GEM-siRRM2 in established cancer xenografts *in vivo*. Tumor growth curves show that NP-sicon and NP-siRRM2 elicited no inhibition of tumor growth in either Panc1-con or Panc1-RRM2 xenografts (Fig. 5C and D). Tumor mass measurements did reveal different inhibitory effects of NP-GEM-sicon treatment in Panc1-con and Panc1-RRM2 xenografts (54% and 22%, respectively) (Fig. 5E). The inhibition in Panc1-RRM2 xenografts treated with NP-GEM-siRRM2 nearly matched that in Panc1-con cells (60% and 57%, respectively; Fig. 5E and Fig. S7), and NP-GEM-siRRM2 treatment induced gene-silence effect against RRM2 in Panc1-RRM2 xenografts (Fig. 5F). Together, these *in vitro* and *in vivo* data indicate that the co-delivery of siRRM2 along with GEM can overcome the low chemosensitivity caused by excessive RRM2 protein expression.

3.6. Therapeutic benefits of NP-GEM-siRRM2 in different patient-derived pancreatic cancer cells depend on the expression levels of hENT1 and RRM2

Primary patient-derived cancer cells were used to study the therapeutic effects of various nanoformulations. Six patient-derived pancreatic cancer cell lines (PDPCs) were established and the expression levels of hENT1 and RRM2 were estimated by immunoblotting (Fig. 6A). We next detected the apoptosis rates of the cultured PDPCs after GEM, NP-GEM-sicon or NP-GEM-siRRM2 treatment (Fig. 6B). Compared to GEM, NP-GEM-sicon induced significantly higher apoptosis rates in all of 6 PDPCs. However, the difference of antitumor efficacy between GEM and NP-GEM-sicon was dramatically elevated in PDPCs with low hENT1 expression (PDPC0019, PDPC0021 and PDPC0045) as compared to that in PDPCs with high hENT1 expression (PDPC0001, PDPC0015 and PDPC0043) (Fig. 6C). The HPLC results also revealed that compared to PDPCs with high hENT1 expression, there were less dFdCTP in cell lysate of PDPCs with low hENT1 expression after GEM treatment, and the intracellular levels of dFdCTP were similar in each PDPC after NP-GEM-sicon treatment (Fig. 6D). In addition, due to the different RRM2 expression level, the increased apoptosis rates of NP-GEM-siRRM2, compared to NP-GEM-sicon, were significantly higher in PDPC0001, PDPC0015 and PDPC0043 than that in PDPC0019, PDPC0021 and PDPC0045 (Fig. 6E). NP-GEM-siRRM2 treatment significantly decrease RRM2 expression in PDPC0001, PDPC0015 and PDPC0043 (Fig. 6F). These data demonstrate that the therapeutic benefits from NP-GEM-sicon and NP-GEM-siRRM2 in different PDPCs were associated with the expression levels of hENT1 and RRM2. NP-GEM-sicon and NP-GEM-siRRM2 can increase the GEM chemosensitivity by overcoming the obstacle caused by low hENT1 expression and high expression of RRM2, respectively.

3.7. Toxicity evaluation of NP and NP-sicon

Next, we examined the cytotoxity *in vitro* and safety *in vivo* of the nanocarrier itself with or without absorbed sicon. The results of CCK-8 assays show that there was a slight cytotoxity 48 h after NP treatment with concentrations greater than 75 μg/ml of the nanocarrier (Fig. S8). The cytotoxity is probably due to the high surface positive charge. Negative control siRNA (sicon)-absorbed NP (NP-sicon), whose surface positive charge is shielded by sicon, exhibited no obvious cytotoxity (Fig. S9). We observed no acute immunological reaction after NP or NP-sicon injection *in vivo* as evidenced by a lack of induction of interferon α (IFN-α), tumor necrosis factor α (TNF-α), or interleukin 6 (IL-6) in the serum of BALB/C mice at 6 h after tail vein injection (Fig. S9). Moreover, after administration of NP or NP-sicon once every 3 days for 20 days, we did not observe any deleterious effects on body weight in mice (Fig. S10A), nor was there any evidence of functional or histological signs of organ toxicity (Figs. S10B and S10C). Collectively, these results are indicative of an excellent safety profile of the nanocarrier for delivering therapeutic agents *in vivo*.

4. Discussion

Several investigations, including the RTOG9704 trial and the ESPAC-3 trial comprising 434 patients [33,34], have found a positive correlation between low expression levels of hENT-1 protein and poor prognosis of post-operation pancreatic cancer patients after GEM treatment. In this study, we detected the expression level of hENT-1 in pancreatic cancer tissue microarray using a validated mouse monoclonal antibody, which is reported to be superior to the rabbit polyclonal antibody [35]. Our results are consistent with these previous findings, further suggesting that hENT1 plays an important role in GEM chemosensitivity. To overcome the low chemosensitivity associated with a lack of hENT1, previous studies synthesized CO-101 (also known as CP-4126), which consists of a molecule of GEM and a molecule of elaidic acid linked by a covalent ester bond [36,37]. The CO-101 enters cells independently of hENT1 because of the elaidic acid. However, in the following phase II

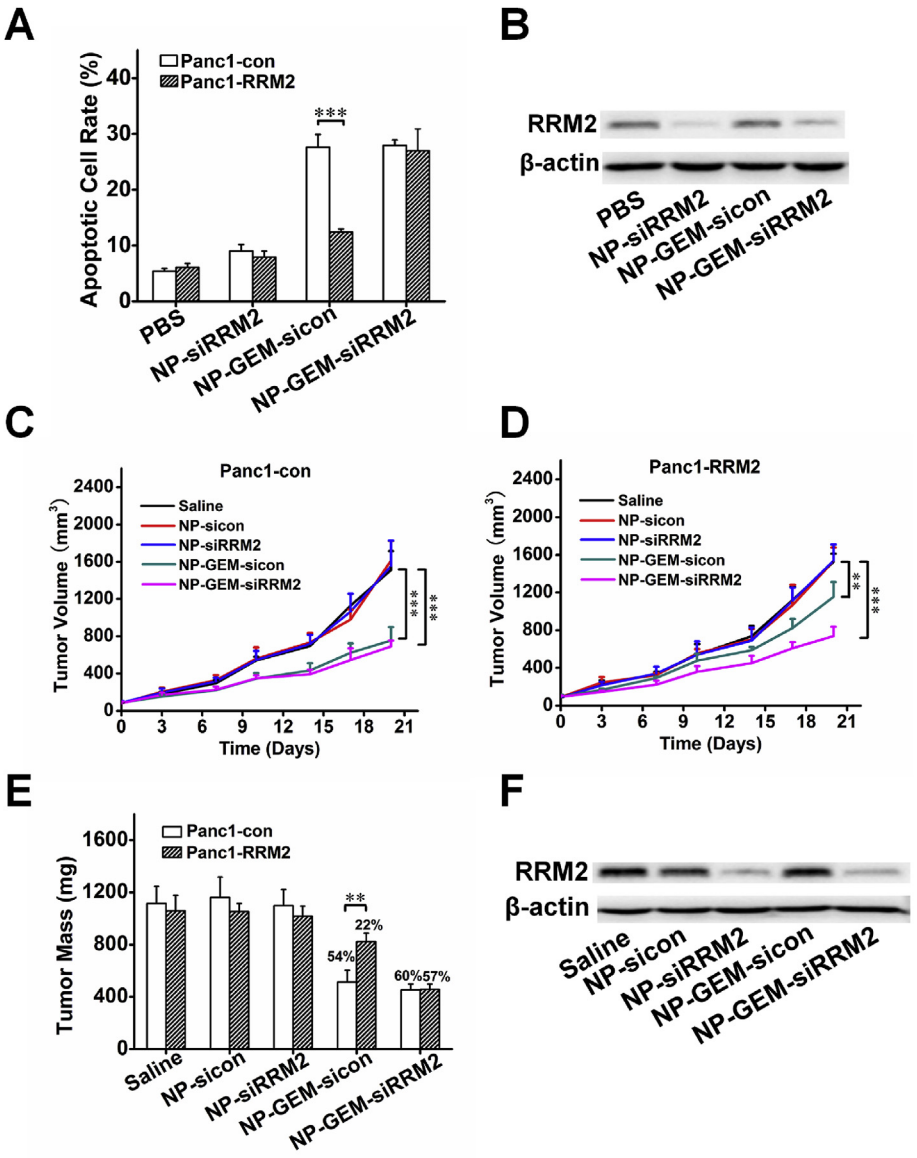

Fig. 5. Co-delivery of siRRM2 significantly enhanced the chemosensitivity of NP-GEM-sicon in pancreatic cancer cells and xenografts with RRM2^{high}. **(A)** The apoptotic cell rate of Panc1-con and Panc1-RRM2 cells after 48 h treatment with different drug formulations. **(B)** Confirmation of RRM2 knockdown in Panc1-RRM2 cells. The proteins of Panc1-RRM2 cells after treatments in panel A were determined by Western blot. **(C, D, E)** The antitumor effects of NP-GEM-siRNA *in vivo*. Mice (n = 5) bearing subcutaneous xenografts of Panc1-con and Panc1-RRM2 were treated with different drug formulations once every 3 days for 20 days. (C and D) The tumor volumes were recorded and plotted against time. (E) Mice were sacrificed at day 20, and tumors were removed and weighed. The inset numbers represent the tumor inhibitory rates in relation to the saline control group. **(F)** The expression of RRM2 in Panc1-RRM2 xenografts after different treatments. $^{**}P < .01$, $^{***}P < .001$.

clinical trial, CO-101 did not exhibit better antitumor effects than GEM, even in the subgroup of patients with low hENT1 expression [38]. One possible reason is that the esterases in human plasma may metabolize CO-101 to GEM before arriving at the tumor site. Our use of a nanocarrier drug delivery strategy to specifically deliver GEM would overcome the issue of plasma activation. In contrast to CO-101 that enter cells *via* elaidic acid, the nanocarrier-encapsulated GEM enters cells as "capsules" containing many GEM molecules, contributing to the higher GEM concentration inside tumor cells. The enhanced drug uptake by tumor cells may account for the ability of the nanoformulations to evade low GEM chemosensitivity because of low hENT1 expression.

A study comprising 95 patients showed that high expression of RRM2 protein was positively associated with reduced RFS and OS after adjutant chemotherapy [39]. On the contrary, another study comprising 117 patients demonstrated that RRM2 protein expression was not predictive of survival from adjuvant GEM treatment after resection [40]. The difference between these two studies is that the former study evaluated RRM2 expression by only nuclear staining, whereas the second study used both cytoplasmic and nuclear staining. In our study, the expression levels of cytosolic RRM2 protein were considered and statistically correlated with RFS and OS. Moreover, some *in vitro* studies reported that RRM2 gene silencing enhances the chemosensitivity of pancreatic cancer cells to GEM [41,42]. Importantly, single treatment using siRNA or inhibitors against RRM2 has been an antitumor therapy in other, non-pancreatic cancer tumors [43–45]. Our results demonstrate that RRM2 silencing alone is insufficient to effectively induce apoptosis of pancreatic cancer cells and inhibit tumor growth *in vivo*, though RRM2 depletion can enhance the efficacy of GEM treatment in

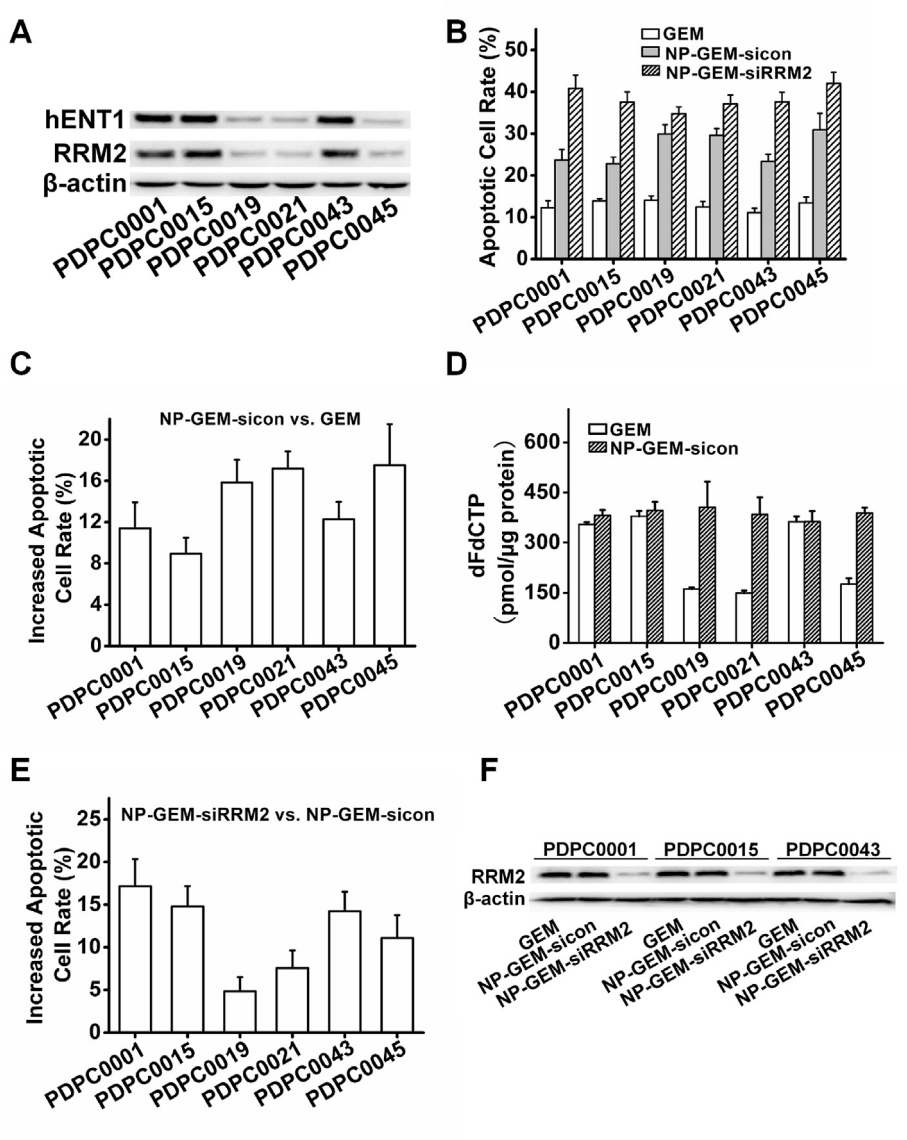

Fig. 6. The cytotoxicity of NP-Gem-sicon and NP-GEM-siRRM2 correlates with the expression levels of hENT1 and RRM2 in primary patient-derived pancreatic cancer cells. **(A)** The expression of hENT1 and RRM2 in the PDPCs as determined by immunoblotting. **(B)** The apoptotic cell rates after GEM, NP-GEM-sicon or NP-GEM-siRRM2 treatment in PDPCs. **(C)** The increase in apoptotic cell rates after NP-GEM-sicon treatment, compared to GEM treatment in different PDPCs. **(D)** The dFdCTP levels in PDPCs lysates detected by HPLC. **(E)** The increase in apoptotic cell rates after NP-GEM-siRRM2 treatment, compared to NP-GEM-sicon treatment in different PDPCs. **(F)** The expression of RRM2 in PDPC0001, PDPC0015 and PDPC0043 after different treatments.

pancreatic cancer cells with RRM2^{high}. There were some controversy reports about the key factors in the GEM chemosensitivity. In our study, the tissue microarray of pathologically identified pancreatic cancer patients was used to evaluate the expression level of four factors in GEM chemosensitivity, and all patients have been confirmed as R0 resection. Tissue microarray has the superiority of consistency compared with the traditional tissue section in previous reports. In addition, the hENT1 antibody in this study was mouse monoclonal antibody, which is reported to be more credible than the rabbit polyclonal antibody in detecting hENT1 expression [35]. In short, we confirmed that hENT1 and RRM2 expression exhibited the important roles in the GEM chemosensitivity in the patients from North China. More importantly, through design of a simple liposome-based GEM and siRRM2 co-delivery system, the GEM resistance due to low hENT1 or high RRM2 expression was overcame effectively.

In this study, the clinical data did not show any relationship between either dCK or RRM1 expression with survival. Previously, two small-scale studies have shown that dCK protein expression may be an important determinant for GEM chemosensitivity [15,46]. There is a variety of studies that have focused on the role of RRM1 in GEM chemosensitivity, but the results are controversal [47–50]. More data is needed to determine the relationship between either dCK or RRM1 expression with GEM chemosensitivity.

Patient-derived tumor cells/xenografts are the most appropriate models for evaluating antitumor drugs in more relevant scenarios [51]. To predict which subpopulation of patients who may obtain therapeutic benefits from our nano-drug formulations, several primary PDPCs were employed in this study. Our data show that the enhancement of antitumor effects of NP-GEM-sicon compared to GEM was higher in PDPCs with hENT1^{low} than that with hENT1^{high}. In addition, compared to NP-GEM-sicon, the benefit from NP-GEM-siRRM2 also correlated with the expression level of RRM2. These results highlight the importance of personalized applications in

nanomedicine, and suggest that the expression levels of genes that were targeted in the design of nano-drug formulations should be evaluated before application.

5. Conclusion

In summary, we found that the essential factors of GEM chemosensitivity in pancreatic cancer patients in North China were the expression levels of hENT1 and RRM2, and synthesized nano-drug formulations can overcome these problems. Moreover, in a series of patient-derived cancer cells, we demonstrated that the therapeutic benefits of the nanomedicine formulations were associated with the expression levels of hENT1 and RRM2. Tailored nano-formulations that overcome the low GEM chemosensitivity provide a new proof-of-concept for the precision and personalized application of nanomedicine in the near future.

Conflicts of interest

The authors declare no competing financial interest.

Acknowledgements

The authors greatly appreciate Professors Saraswati Sukumar and Kam W. Leong for their constructive suggestions. The primary patient-derived pancreatic cancer cells were provided by WuXiAppTec Co., Ltd. in China. This work was supported by the National Distinguished Young Scientists program (31325010), the Innovation Research Group of National Natural Science Foundation (11621505), the Key Research Project of Frontier science of the Chinese Academy of Sciences (QYZDJ-SSW-SLH022), the Key Research Program of the Chinese Academy of Sciences (KGZD-EW-T06), the National Postdoctoral Program for Innovative Talents (BX201600042), the Chinese Postdoctoral Science Foundation (2017M610839), the National Natural Science Foundation of China (51673051, 81672431, 81672435, 31300822, 91543127, 81525021, 81502067, 81572618, 31471340 and 31470957), and Academy of Medical Sciences-Newton Advanced Fellowship.

Appendix A. Supplementary data

Supplementary data related to this article can be found at https://doi.org/10.1016/j.biomaterials.2017.12.015.

References

[1] S. Farber, L.K. Diamond, Temporary remissions in acute leukemia in children produced by folic acid antagonist, 4-aminopteroyl-glutamic acid, N. Engl. J. Med. 238 (1948) 787–793.
[2] C.M. Stevens, A. Mylorie, C. Auerbach, H. Moser, I. Kirk, K.A. Jensen, et al., Biological action of 'mustard gas' compounds, Nature 166 (1950) 1019–1021.
[3] R. Perez-Tomas, Multidrug resistance: retrospect and prospects in anti-cancer drug treatment, Curr. Med. Chem. 13 (2006) 1859–1876.
[4] D.P. Ryan, T.S. Hong, N. Bardeesy, Pancreatic adenocarcinoma, N. Engl. J. Med. 371 (2014) 1039–1049.
[5] A. Vincent, J. Herman, R. Schulick, R.H. Hruban, M. Goggins, Pancreatic cancer, Lancet 378 (2011) 607–620.
[6] T. Conroy, F. Desseigne, M. Ychou, O. Bouche, R. Guimbaud, Y. Becouarn, et al., FOLFIRINOX versus gemcitabine for metastatic pancreatic cancer, N. Engl. J. Med. 364 (2011) 1817–1825.
[7] R. Agarwal, S.B. Kaye, Ovarian cancer: strategies for overcoming resistance to chemotherapy, Nat. Rev. Canc. 3 (2003) 502–516.
[8] A. Ganoth, K.C. Merimi, D. Peer, Overcoming multidrug resistance with nanomedicines, Expet Opin. Drug Deliv. 12 (2015) 223–238.
[9] T. Ji, S. Li, Y. Zhang, J. Lang, Y. Ding, X. Zhao, et al., An MMP-2 responsive liposome integrating antifibrosis and chemotherapeutic drugs for enhanced drug perfusion and efficacy in pancreatic cancer, ACS Appl Mater Interfaces 8 (2016) 3438–3445.
[10] Y. Nakano, S. Tanno, K. Koizumi, T. Nishikawa, K. Nakamura, M. Minoguchi, et al., Gemcitabine chemoresistance and molecular markers associated with gemcitabine transport and metabolism in human pancreatic cancer cells, Br J Canc. 96 (2007) 457–463.
[11] J. Garcia-Manteiga, M. Molina-Arcas, F.J. Casado, A. Mazo, M. Pastor-Anglada, Nucleoside transporter profiles in human pancreatic cancer cells: role of hCNT1 in 2',2'-difluorodeoxycytidine- induced cytotoxicity, Clin. Canc. Res. 9 (2003) 5000–5008.
[12] J.R. Mackey, R.S. Mani, M. Selner, D. Mowles, J.D. Young, J.A. Belt, et al., Functional nucleoside transporters are required for gemcitabine influx and manifestation of toxicity in cancer cell lines, Canc. Res. 58 (1998) 4349–4357.
[13] S. Ohhashi, K. Ohuchida, K. Mizumoto, H. Fujita, T. Egami, J. Yu, et al., Down-regulation of deoxycytidine kinase enhances acquired resistance to gemcitabine in pancreatic cancer, Anticancer Res. 28 (2008) 2205–2212.
[14] A.W. Blackstock, H. Lightfoot, L.D. Case, J.E. Tepper, S.K. Mukherji, B.S. Mitchell, et al., Tumor uptake and elimination of 2',2'-difluoro-2'-deoxycytidine (gemcitabine) after deoxycytidine kinase gene transfer: correlation with in vivo tumor response, Clin. Canc. Res. 7 (2001) 3263–3268.
[15] V. Sebastiani, F. Ricci, B. Rubio-Viqueira, P. Kulesza, C.J. Yeo, M. Hidalgo, et al., Immunohistochemical and genetic evaluation of deoxycytidine kinase in pancreatic cancer: relationship to molecular mechanisms of gemcitabine resistance and survival, Clin. Canc. Res. 12 (2006) 2492–2497.
[16] N.M. Cerqueira, P.A. Fernandes, M.J. Ramos, Understanding ribonucleotide reductase inactivation by gemcitabine, Chemistry 13 (2007) 8507–8515.
[17] W. Plunkett, P. Huang, C.E. Searcy, V. Gandhi, Gemcitabine: preclinical pharmacology and mechanisms of action, Semin. Oncol. 23 (1996) 3–15.
[18] S. Eriksson, D.W. Martin Jr., Ribonucleotide reductase in cultured mouse lymphoma cells. Cell cycle-dependent variation in the activity of subunit protein M2, J. Biol. Chem. 256 (1981) 9436–9440.
[19] J. Herrick, B. Sclavi, Ribonucleotide reductase and the regulation of DNA replication: an old story and an ancient heritage, Mol. Microbiol. 63 (2007) 22–34.
[20] E. Giovannetti, M. Del Tacca, V. Mey, N. Funel, S. Nannizzi, S. Ricci, et al., Transcription analysis of human equilibrative nucleoside transporter-1 predicts survival in pancreas cancer patients treated with gemcitabine, Canc. Res. 66 (2006) 3928–3935.
[21] J. Spratlin, R. Sangha, D. Glubrecht, L. Dabbagh, J.D. Young, C. Dumontet, et al., The absence of human equilibrative nucleoside transporter 1 is associated with reduced survival in patients with gemcitabine-treated pancreas adenocarcinoma, Clin. Canc. Res. 10 (2004) 6956–6961.
[22] H. Fujita, K. Ohuchida, K. Mizumoto, S. Itaba, T. Ito, K. Nakata, et al., Gene expression levels as predictive markers of outcome in pancreatic cancer after gemcitabine-based adjuvant chemotherapy, Neoplasia 12 (2010) 807–817.
[23] Y. Nakano, S. Tanno, K. Koizumi, T. Nishikawa, K. Nakamura, M. Minoguchi, et al., Gemcitabine chemoresistance and molecular markers associated with gemcitabine transport and metabolism in human pancreatic cancer cells, Br J Canc. 96 (2007) 457–463.
[24] R. Ashida, B. Nakata, M. Shigekawa, N. Mizuno, A. Sawaki, K. Hirakawa, et al., Gemcitabine sensitivity-related mRNA expression in endoscopic ultrasound-guided fine-needle aspiration biopsy of unresectable pancreatic cancer, J. Exp. Clin. Canc. Res. 28 (2009) 83.
[25] J. Bai, N. Sata, H. Nagai, Gene Expression Analysis for Predicting Gemcitabine Sensitivity in Pancreatic Cancer Patients, HPB (Oxford), vol. 9, 2007, pp. 150–155.
[26] R. Andersson, U. Aho, B.I. Nilsson, G.J. Peters, M. Pastor-Anglada, W. Rasch, et al., Gemcitabine chemoresistance in pancreatic cancer: molecular mechanisms and potential solutions, Scand. J. Gastroenterol. 44 (2009) 782–786.
[27] D. Peer, J.M. Karp, S. Hong, O.C. FaroKHzad, R. Margalit, R. Langer, Nanocarriers as an emerging platform for cancer therapy, Nat. Nanotechnol. 2 (2007) 751–760.
[28] M. Ferrari, Cancer nanotechnology: opportunities and challenges, Nat. Rev. Canc. 5 (2005) 161–171.
[29] S. Kapse-Mistry, T. Govender, R. Srivastava, M. Yergeri, Nanodrug delivery in reversing multidrug resistance in cancer cells, Front. Pharmacol. 5 (2014) 159.
[30] X. Zhao, F. Li, Y.Y. Li, H. Wang, H. Ren, J. Chen, et al., Co-delivery of HIF1 alpha siRNA and gemcitabine via biocompatible lipid-polymer hybrid nanoparticles for effective treatment of pancreatic cancer, Biomaterials 46 (2015) 13–25.
[31] F. Li, X. Zhao, H. Wang, R.F. Zhao, T.J. Ji, H. Ren, et al., Multiple layer-by-layer lipid-polymer hybrid nanoparticles for improved Folfirinox chemotherapy in pancreatic tumor models, Adv. Funct. Mater. 25 (2015) 788–798.
[32] I. Koltover, T. Salditt, J.O. Rädler, C.R. Safinya, An inverted hexagonal phase of cationic liposome-DNA complexes related to DNA release and delivery, Science 281 (1998) 78–81.
[33] J.J. Farrell, H. Elsaleh, M. Garcia, R. Lai, A. Ammar, W.F. Regine, et al., Human equilibrative nucleoside transporter 1 levels predict response to gemcitabine in patients with pancreatic cancer, Gastroenterology 136 (2009) 187–195.
[34] W. Greenhalf, P. Ghaneh, J.P. Neoptolemos, D.H. Palmer, T.F. Cox, R.F. Lamb, et al., Pancreatic cancer hENT1 expression and survival from gemcitabine in patients from the ESPAC-3 trial, J Natl Cancer Inst 106 (2014) djt347.
[35] M. Svrcek, J. Cros, R. Marechal, J.B. Bachet, J.F. Flejou, P. Demetter, Human equilibrative nucleoside transporter 1 testing in pancreatic ductal adenocarcinoma: a comparison between murine and rabbit antibodies, Histopathology 66 (2015) 457–462.
[36] A.D. Adema, K. Smid, N. Losekoot, R.J. Honeywell, H.M. Verheul, F. Myhren, et al., Metabolism and accumulation of the lipophilic deoxynucleoside analogs elacytarabine and CP-4126, Invest. N. Drugs 30 (2012) 1908–1916.
[37] A.M. Bergman, A.D. Adema, J. Balzarini, S. Bruheim, I. Fichtner, P. Noordhuis, et

al., Antiproliferative activity, mechanism of action and oral antitumor activity of CP-4126, a fatty acid derivative of gemcitabine, in in vitro and in vivo tumor models, Invest. N. Drugs 29 (2011) 456–466.
[38] E. Poplin, H. Wasan, L. Rolfe, M. Raponi, T. Ikdahl, I. Bondarenko, et al., Randomized, multicenter, phase II study of CO-101 versus gemcitabine in patients with metastatic pancreatic ductal adenocarcinoma: including a prospective evaluation of the role of hENT1 in gemcitabine or CO-101 sensitivity, J. Clin. Oncol. 31 (2013) 4453–4461.
[39] S.B. Fisher, S.H. Patel, P. Bagci, D.A. Kooby, B.F. El-Rayes, C.A. Staley 3rd, et al., An analysis of human equilibrative nucleoside transporter-1, ribonucleoside reductase subunit M1, ribonucleoside reductase subunit M2, and excision repair cross-complementing gene-1 expression in patients with resected pancreas adenocarcinoma: implications for adjuvant treatment, Cancer 119 (2013) 445–453.
[40] H. Xie, J. Lin, D.G. Thomas, W. Jiang, X. Liu, Ribonucleotide reductase M2 does not predict survival in patients with resectable pancreatic adenocarcinoma, Int. J. Clin. Exp. Pathol. 5 (2012) 347–355.
[41] M.S. Duxbury, H. Ito, E. Benoit, M.J. Zinner, S.W. Ashley, E.E. Whang, Retrovirally mediated RNA interference targeting the M2 subunit of ribonucleotide reductase: a novel therapeutic strategy in pancreatic cancer, Surgery 136 (2004) 261–269.
[42] M.S. Duxbury, H. Ito, M.J. Zinner, S.W. Ashley, E.E. Whang, RNA interference targeting the M2 subunit of ribonucleotide reductase enhances pancreatic adenocarcinoma chemosensitivity to gemcitabine, Oncogene 23 (2004) 1539–1548.
[43] N.M. Cerqueira, S. Pereira, P.A. Fernandes, M.J. Ramos, Overview of ribonucleotide reductase inhibitors: an appealing target in anti-tumour therapy, Curr. Med. Chem. 12 (2005) 1283–1294.
[44] J.D. Heidel, J.Y. Liu, Y. Yen, B. Zhou, B.S. Heale, J.J. Rossi, et al., Potent siRNA inhibitors of ribonucleotide reductase subunit RRM2 reduce cell proliferation in vitro and in vivo, Clin. Canc. Res. 13 (2007) 2207–2215.
[45] M.E. Davis, J.E. Zuckerman, C.H. Choi, D. Seligson, A. Tolcher, C.A. Alabi, et al., Evidence of RNAi in humans from systemically administered siRNA via targeted nanoparticles, Nature 464 (2010) 1067–1070.
[46] R. Marechal, J.R. Mackey, R. Lai, P. Demetter, M. Peeters, M. Polus, et al., Deoxycitidine kinase is associated with prolonged survival after adjuvant gemcitabine for resected pancreatic adenocarcinoma, Cancer 116 (2010) 5200–5206.
[47] R. Marechal, J.B. Bachet, J.R. Mackey, C. Dalban, P. Demetter, K. Graham, et al., Levels of gemcitabine transport and metabolism proteins predict survival times of patients treated with gemcitabine for pancreatic adenocarcinoma, Gastroenterology 143 (2012) 664–674 e666.
[48] N. Nakagawa, Y. Murakami, K. Uemura, T. Sudo, Y. Hashimoto, N. Kondo, et al., Combined analysis of intratumoral human equilibrative nucleoside transporter 1 (hENT1) and ribonucleotide reductase regulatory subunit M1 (RRM1) expression is a powerful predictor of survival in patients with pancreatic carcinoma treated with adjuvant gemcitabine-based chemotherapy after operative resection, Surgery 153 (2013) 565–575.
[49] H. Akita, Z. Zheng, Y. Takeda, C. Kim, N. Kittaka, S. Kobayashi, et al., Significance of RRM1 and ERCC1 expression in resectable pancreatic adenocarcinoma, Oncogene 28 (2009) 2903–2909.
[50] M.E. Valsecchi, T. Holdbrook, B.E. Leiby, E. Pequignot, S.J. Littman, C.J. Yeo, et al., Is there a role for the quantification of RRM1 and ERCC1 expression in pancreatic ductal adenocarcinoma? BMC Canc. 12 (2012) 104.
[51] D. Siolas, G.J. Hannon, Patient-derived tumor xenografts: transforming clinical samples into mouse models, Canc. Res. 73 (2013) 5315–5319.